

Research Article pubs.acs.org/acscatalysis

Photocatalytic Pinacol C—C Coupling and Jet Fuel Precursor Production on ZnIn₂S₄ Nanosheets

Guanqun Han, Xingwu Liu, Zhi Cao, and Yujie Sun*



Cite This: ACS Catal. 2020, 10, 9346-9355



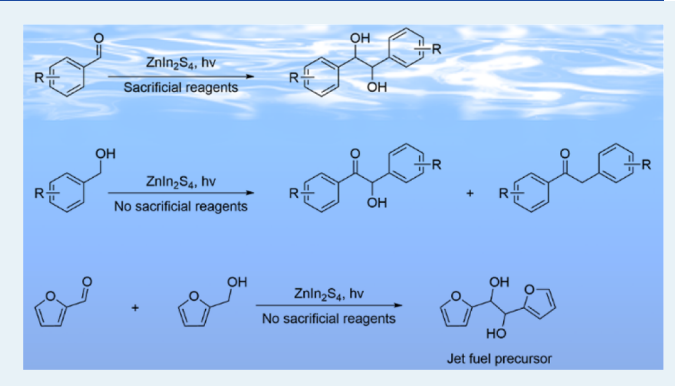
ACCESS I

Metrics & More

Article Recommendations

Supporting Information

ABSTRACT: Visible light-driven C-C bond formation has attracted increasing attention recently, thanks to the advance in molecular photosensitizers and organometallic catalysts. Nevertheless, these homogeneous methodologies typically necessitate the utilization of noble metal-based (e.g., Ir, Ru, etc.) photosensitizers. In contrast, solid-state semiconductors represent an attractive alternative but remain less explored for C-C bondforming reactions driven by visible-light irradiation. Herein, we report that photocatalytic pinacol C-C coupling of benzaldehyde to hydrobenzoin can be achieved on two-dimensional ZnIn₂S₄ nanosheets upon visible-light irradiation in the presence of a sacrificial electron donor (e.g., triethylamine). We further demonstrate that it is feasible to take advantage of both excited



electrons and holes in irradiated ZnIn₂S₄ for C-C coupling reactions in the absence of any sacrificial reagent if benzyl alcohol is utilized as the starting substrate, maximizing the energy efficiency of photocatalysis and circumventing any byproducts. In this case, industrially important benzoin and deoxybenzoin are formed as the final products. More importantly, by judiciously tuning the photocatalytic conditions, we are able to produce either benzoin or deoxybenzoin with unprecedented high selectivity. The critical species during the photocatalytic process were systematically investigated with various scavengers. Finally, such a heterogeneous photocatalytic pinacol C-C coupling strategy was applied to produce a jet fuel precursor (e.g., hydrofuroin) from biomass-derived furanics (e.g., furfural and furfural alcohol), highlighting the promise of our approach in practical applications.

KEYWORDS: photocatalysis, C-C coupling, semiconductor, biomass valorization, jet fuel precursor

INTRODUCTION

The development of atom-economic and step-efficient C-C bond formation has long been one of the central themes in organic synthesis. The last century has witnessed a great advance in C-C bond-forming strategies thanks to many elegant molecular catalysts consisting of transition-metal complexes. 1-3 These homogeneous C-C coupling strategies demonstrate outstanding functional group tolerance, wide versatility, high yield, and excellent selectivity; hence, they have become an essential tool kit in the arsenal of organic chemists. Nevertheless, a common drawback of these classical C-C coupling reactions is that they typically require substrates with leaving groups (e.g., halogen, alkylsilyl, boronic acid, and carboxylate substituents) and expensive reagents and produce stoichiometric/toxic byproducts. The overall atom economy of these C-C coupling strategies is rather mediocre. Following the principles of green chemistry, it is highly desirable to explore more atom-economic and step-efficient C-C bondforming approaches under ambient conditions with less or no byproducts. Within this context, pinacol C-C coupling of carbonyls and alcohols stands out as a promising approach, especially when it can be accomplished under ambient

conditions with green energy input such as visible-light irradiation.

Carbonyls and alcohols are among the most ubiquitous functionalities in organic molecules. Ketyl radicals generated from carbonyls through umpolung (polarity reversal) of the carbon-oxygen double bonds can initiate C-C bond formation. However, because of the higher activation-energy barrier, strong reducing agents, such as Sm^{II}, Ti^{II}, Zn, Mn, Mg, Al, and so forth, are required for the umpolung of carbonyl groups. 4-8 Unfortunately, the use of stoichiometric equivalent of strong reducing agents poses severe issues of air sensitivity, functional-group tolerance, unwanted side reactions, and a large quantity of unavoidable waste products.

Hence, a greener and catalytic strategy is very appealing. Arguably, the greenest driving force for a chemical reaction is

Received: April 16, 2020 Revised: July 7, 2020 Published: July 28, 2020





light. It is well recognized that molecular photosensitizers have emerged as a powerful tool in organic synthesis during the last 2 decades. Indeed, photocatalytic generation of ketyl radicals from carbonyls following a proton-coupled electron transfer (PCET) process is a manifestation of the power of organic photocatalysis. ^{9–17} For instance, Rueping et al. reported that an alkyl ammine can be oxidized by an excited Ir-based photosensitizer to yield an α -ammonium radical which can act as a hydrogen bond activator to induce the umpolung of carbonyls to generate ketyl radicals via a PCET step. ¹⁸ The produced ketyl radicals dimerize to form desired diol products.

Nevertheless, those homogeneous photocatalytic approaches usually require expensive molecular photosensitizers, many of which contain high-cost noble metals such as Ir and Ru. Second, the requirement of sacrificial reagents which are used in large excess inevitably leads to a large amount of byproducts. These byproducts are not only hard to be separated from those desirable products but also undergo unclear degradation pathways, posing environmental concerns. In contrast, heterogeneous semiconductor-based photocatalytic systems offer an alternative approach due to their relatively easier preparation, potentially lower cost, and straightforward separation (phase separation) and recyclability. Additionally, two-half reactions (oxidation and reduction) can be potentially achieved simultaneously utilizing one semiconductor. 19-Along with the rapidly increasing interest in energy catalysis, particularly in the fields of solar-energy capture, conversion, and storage, semiconductor-based photocatalytic systems have been frequently investigated for small-molecule activation and transformation reactions. ^{22–25} However, most reported semiconductor systems for photocatalytic pinacol coupling are only UV-light responsive. Only recently, a few elegant works utilizing visible-light irradiation for pinacol coupling have emerged.³⁰⁻³³ For instance, McClelland and Weiss reported the visible light-driven transformation of benzyl alcohol to C-C coupled products on CdS quantum dots.³⁰ Unfortunately, a mixture of hydrobenzoin, deoxybenzoin, and benzil with poor selectivity was obtained. Wang et al. reported the generation of benzoin or deoxybenzoin with mediocre yields of 61 or 64% together with low selectivity of each product.3

It is necessary to mention that hydrobenzoin, benzoin, and deoxybenzoin are all useful commodity chemicals. Hydrobenzoin and its derivatives have a wide range of applications in fine synthesis (particularly in chiral chemistry). Benzoin is an important feedstock for the synthesis of a variety of value-added chemicals, including additives, dyestuff, photoinitiator precursors, and pharmaceuticals. Deoxybenzoin is an important precursor for the synthesis of carbocycles, heterocycles, and a large number of natural products with biological activities. However, it is a challenge to realize the production of hydrobenzoin, benzoin, or deoxybenzoin from pinacol C–C coupling with very high selectivity, not even to mention on one semiconductor with visible-light irradiation.

Our group has initiated a program focusing on organic transformations via semiconductor-based photocatalysts. Herein, we report a ketyl radical-initiated C–C coupling reaction on semiconductors from three aspects (Scheme 1). (i) C–C bond formation from benzaldehyde to hydrobenzoin is achieved via two-dimensional $ZnIn_2S_4$ nanosheets with the aid of a sacrificial electron donor, triethylamine (TEA). (ii) In order to circumvent the use of sacrificial reagents and maximize the utilization of both excited electrons and holes of the semiconductor, benzyl alcohol is employed to realize C–C

Scheme 1. Our Approach Utilizing $ZnIn_2S_4$ as a Photocatalyst for Pinacol Coupling Reactions and Its Application in the Production of a Jet Fuel Precursor from Biomass-Derived Furanics

Approach: photocatalytic pinacol coupling with/without sacrificial reagent.

Application: production of a jet fuel precursor from biomass-derived molecules.

coupling in the absence of any sacrificial reagents. By judiciously tuning reaction conditions, synthesis of benzoin and deoxybenzoin with unprecedented high selectivity is obtained. (iii) We further demonstrate the application of this ketyl radical-initiated C—C coupling strategy in the production of a biofuel precursor, hydrofuroin, from the homocoupling of furfural. Furfural is a biomass-derived platform chemical, and its dimerization product hydrofuroin, a C10 compound, can act as a jet fuel precursor.

■ RESULT AND DISCUSSION

ZnIn₂S₄ was selected as our target semiconductor because of its suitable band structure not only exhibiting visible-light absorption but also encompassing a wide redox potential window. 41-43 A microwave-assisted solvothermal method was developed in our group to synthesize ZnIn₂S₄ in a very timeefficient manner. A variety of ZnIn₂S₄ samples could be readily synthesized at different temperatures, and the one obtained at 120 °C was characterized thoroughly because of its optimal photocatalytic performance (see Result and Discussion in later sections). X-ray diffraction (XRD) characterization of ZnIn₂S₄ confirms its hexagonal crystal structure (JCPDS: 03-065-2023)⁴⁴ (Figure 1a), and its scanning electron microscopy (SEM) image indicates a nanosheet morphology (Figure 1b), which is further confirmed by transmission electron microscopy (TEM) (Figure 1c). High-resolution TEM (HRTEM) image shows clear lattice fringes of 0.322 nm and 0.293 nm, which belong to (102) and (104) crystal planes of hexagonal ZnIn₂S₄ (Figure 1d). TEM elemental mapping images of ZnIn₂S₄ are presented in Figure 1e, demonstrating the uniform distribution of Zn, In, and S in the entire sample, and atomic ratio of Zn/In/S is close to 1:2:4 (Figure S1). In addition, the survey and high-resolution X-ray photoelectron spectroscopy (XPS) results are plotted in Figures S2 and 1f, respectively. Those most prominent peaks observed at 1022.1, 445.1, and

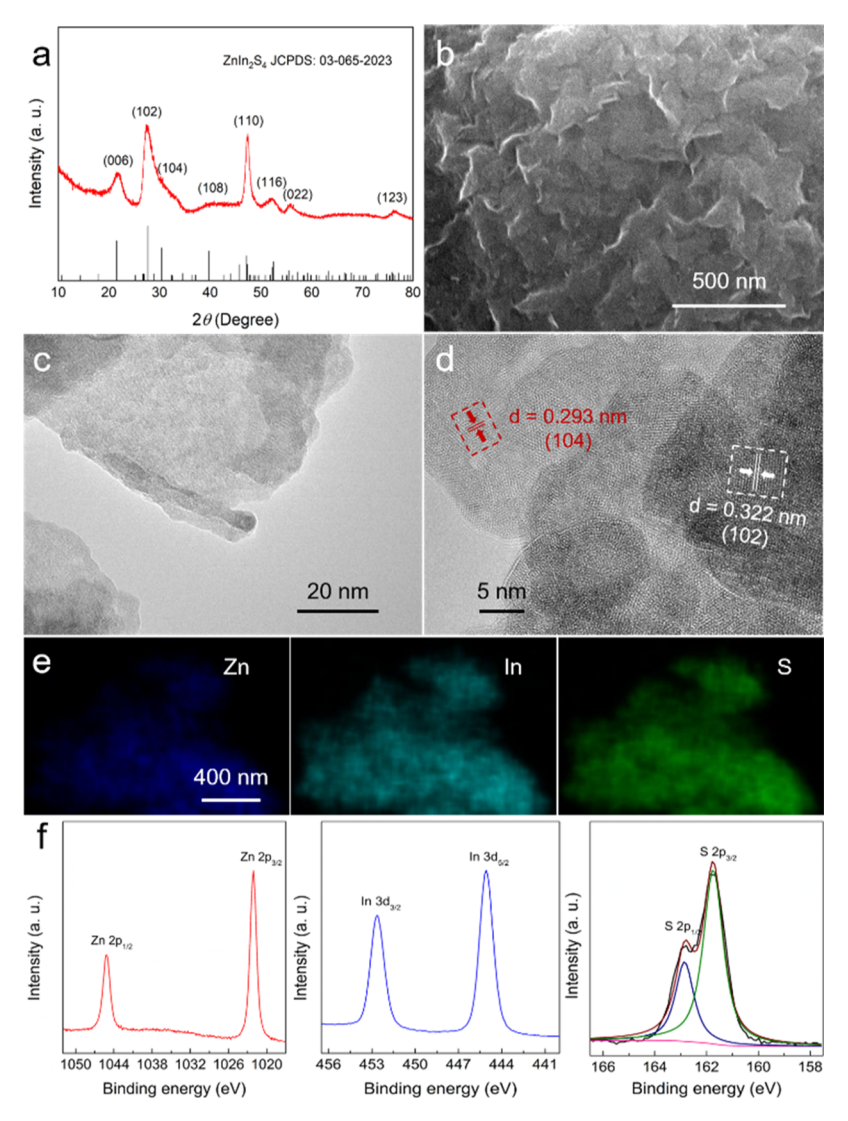


Figure 1. Physical characterization results of synthesized ZnIn₂S₄. (a) XRD together with its standard pattern (JCPDS: 03-065-2023), (b) SEM, (c) TEM, (d) HRTEM, and (e) TEM elemental mapping images of ZnIn₂S₄. (f) High-resolution XPS spectra of Zn, In, and S in ZnIn₂S₄.

161.7 eV are assigned to Zn $2p_{3/2}$, In $3d_{5/2}$, and S $2p_{3/2}$ features, respectively. The spin orbit separation for each element are 23.0, 7.5, and 1.2 eV for Zn 2p, In 3d, and S 2p spectra, respectively. Furthermore, the ratios of those two peaks in each spectrum are 1:2 (Zn 2p), 2:3 (In 3d), and 1:2 (S 2p), which are well consistent with the anticipated valence states of Zn^{2+} , In^{3+} , and S^{2-} in $ZnIn_2S_4$.

Photocatalytic homocoupling of benzaldehyde in the presence of TEA was adopted as the initial reaction to screen the activity of synthesized ZnIn₂S₄ candidates. A series of 2 h photocatalysis in acetonitrile using ZnIn₂S₄ prepared at 80, 90, 100, 110, 120, and 130 °C demonstrates that the semiconductor obtained at 120 °C exhibited the highest benzaldehyde conversion as well as the highest yield of the desirable C–C coupling product, hydrobenzoin (Table S1, entry 1–6). Therefore, all of the following experiments were conducted using ZnIn₂S₄ synthesized at 120 °C unless noted otherwise. Control experiments performed in the absence of either one of the following items, light, catalyst, and TEA prove their necessity in achieving C–C coupling of benzaldehyde (Table S1, entry 7–9). It was also noticed that the addition of water would apparently result in an improvement in both

benzaldehyde conversion and hydrobenzoin yield (Table S1, entry 10-13). For instance, 10% (v/v) water in acetonitrile led to the 100% conversion of benzaldehyde within 2 h photocatalysis and the yield of hydrobenzoin (79%) was also higher than that obtained in pure acetonitrile (49%). Once the water volume percentage was larger than 70%, nearly quantitative hydrobenzoin could be obtained.

In order to gain more insights of the reaction kinetics in different solvent mixtures, the concentration evolution of benzaldehyde, hydrobenzoin, and the side-product benzyl alcohol was quantified via high-performance liquid chromatography (HPLC). The concentration of each compound was calculated based on their corresponding calibration curves (Figures S3 and S4). Figure 2a plots the conversion profile of benzaldehyde, while Figure 2b shows the yields of hydrobenzoin and benzyl alcohol over time in different solvent mixtures of acetonitrile and water. Their HPLC traces are included in Figure S5. It is apparent that in pure acetonitrile, even after 4 h photocatalysis, the conversion of benzaldehyde was only \sim 80% and the yield of hydrobenzoin was \sim 70%. However, upon the addition of water, the consumption of benzaldehyde was much faster and the yield of hydrobenzoin

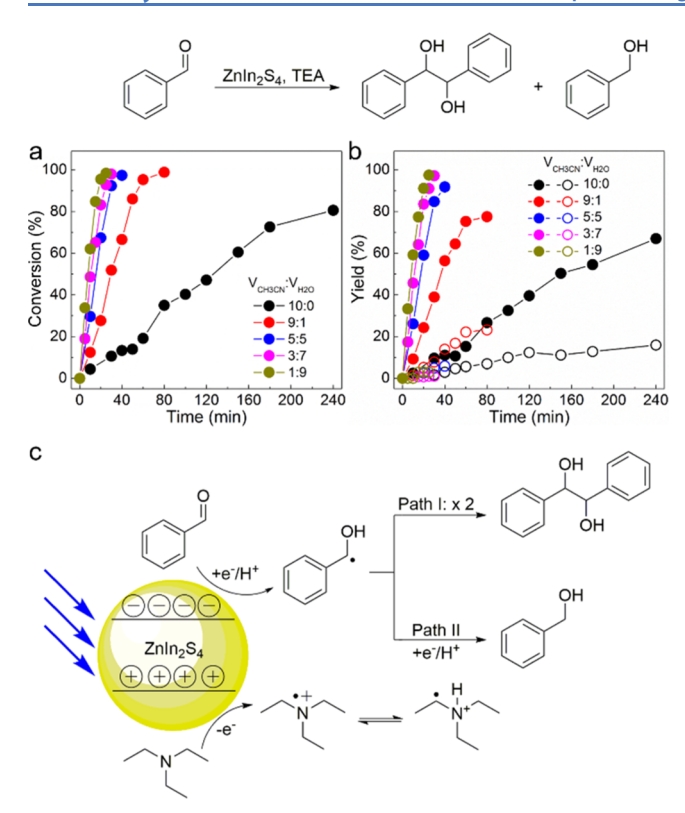


Figure 2. Photocatalytic coupling of benzaldehyde. (a) Benzaldehyde conversion and (b) yields of hydrobenzoin (solid sphere) and benzyl alcohol (hollow sphere) over time [condition: 10 mM benzaldehyde, 1 mL TEA, 10 mg ZnIn₂S₄, room temperature, 10 mL mixture solvent of CH₃CN/H₂O (volume ratios shown as legends), blue LED]. (c) Postulated reaction pathways from benzaldehyde to hydrobenzoin and benzyl alcohol.

also rapidly increased. It should be noted that in CH_3CN/H_2O (v/v: 1/9), benzaldehyde was almost completely converted to hydrobenzoin within half an hour photocatalysis using our $ZnIn_2S_4$ photocatalyst (Figure S6).

A control experiment conducted in CH₃CN/D₂O demonstrated that there was no deuterium atom incorporated in the final product hydrobenzoin fragment, implying that the hydrogen source might not be water but TEA (Figure S7). This observation is in agreement with the previous reports.⁴⁷ However, the occurrence of isotope exchange between the hydroxyl group of hydrobenzoin and D₂O cannot be excluded. A plausible reaction scheme is postulated in Figure 2c. Upon light irradiation, the generated excited hole in ZnIn₂S₄ oxidizes TEA to a radical cation, which is able to release a proton (H⁺) to the semiconductor surface, resulting in a hydrogen pool. 48 In the meantime, benzaldehyde is reduced by the excited electron of ZnIn₂S₄ and an overall PCET step produces the critical ketyl radical. If the concentration of ketyl radical is high on the semiconductor surface, radical homocoupling will take place and the desirable hydrobenzoin will be formed. However, if hydrogen (H*) is captured by the ketyl radical, benzyl alcohol will be produced. The lower solubility of benzaldehyde in water relative to that in acetonitrile likely induces higher concentration of ketyl radical on the ZnIn₂S₄ surface once more water is added to the reaction solution, hence leading to higher yield and selectivity of hydrobenzoin.

We next explored the versatility of this homocoupling strategy to other benzaldehyde derivatives. In order to maintain reasonable solubility of these aromatic substrates in the photocatalysis solution, a mixture of CH_3CN/H_2O (v/v: 3/7) was utilized for all of the following experiments. As tabulated in Table 1, all electron-withdrawing substituents

Table 1. Photocatalytic C—C Coupling of Benzaldehyde and Its Derivatives^a

"Condition: 10 mM aldehyde substrate, 1 mL TEA, 10 mg of $ZnIn_2S_4$, 3 mL of CH_3CN , 7 mL of H_2O , blue LED, 0.5 h (6 h for yield shown in parenthesis).

(-CN, -CF₃, -F, and -Cl) at the para position of the benzene ring resulted in nearly quantitative conversion of the parent aldehydes to the final C-C coupling products with nearly unity yields within 0.5 h photocatalysis (Figures S8–S11), in agreement with the fact that electron-withdrawing groups render the aldehyde group easier to be reduced and favor the formation of ketyl radicals. On the other hand, the presence of electron-donating substituents inevitably lowered the yield and selectivity of the C-C coupling products (Figures S12 and S13) because of the more negative reduction potential of their aldehyde groups and thus slow the formation of the critical ketyl radicals on the ZnIn₂S₄ surface.

The above photocatalytic C-C coupling of benzaldehyde still requires the utilization of a sacrificial electron donor, TEA, which wastes the oxidation power of excited holes in ZnIn₂S₄ upon irradiation and leads to inevitable byproducts. It would be more appealing if both excited electrons and holes of the semiconductor photocatalyst could be utilized to drive C-C bond formation reactions in the absence of sacrificial reagents and produce no byproducts. Given the oxidation power of the valence band in ZnIn₂S₄, we anticipated it would be able to oxidize benzyl alcohol and yield a ketyl radical as an intermediate. It is expected that two reaction pathways can take place following the formation of the in situ formed ketyl radical. Pathway I involves a second oxidation step and results in benzaldehyde and H2. However, as demonstrated earlier, benzaldehyde can be further reduced to initiate the C-C coupling process. On the other hand, if the initially formed ketyl radicals appear in high concentration on the ZnIn₂S₄ surface, they can homocouple to produce hydrobenzoin immediately (pathway II). Because no sacrificial electron donors are present in the reaction solution, there is a possibility that the newly formed hydrobenzoin would be further oxidized during photocatalysis. Indeed, as plotted in Figures 3, S14, and S15, benzoin and deoxybenzoin were

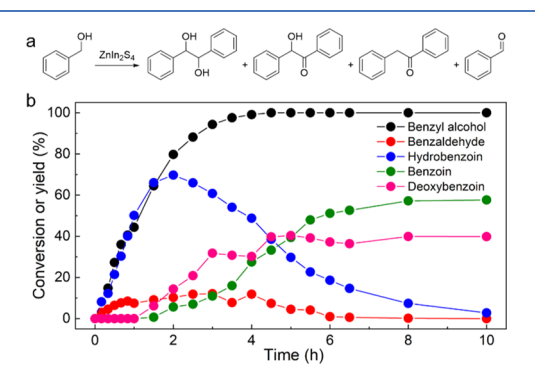


Figure 3. Photocatalytic coupling of benzyl alcohol. (a) Plausible reaction of photocatalytic C–C coupling reactions using benzyl alcohol as the starting substrate. (b) Conversion of benzyl alcohol and yields of products over time during photocatalysis. Condition: 10 mM benzyl alcohol, 10 mg ZnIn₂S₄, 3 mL CH₃CN, 7 mL H₂O, blue LED.

detected as the final major products with yields of 58 and 40%, respectively, together with the formation of additional H₂ (Figure S16). Therefore, the overall yield of C-C coupling products was 98%. Hydrobenzoin was formed as an intermediate with a maximum yield of ~70% reached within 2 h of photocatalysis and continuous irradiation led to its consumption and rise of benzoin and deoxybenzoin. It should be noted that benzaldehyde was indeed detected during the entire photocatalysis period; however, its yield remained low $(\sim 10\%)$ during the first 5 h and nearly disappeared in the second half of photocatalysis. Heterocoupling between benzyl alcohol and benzaldehyde was conducted as a control experiment. After photocatalysis, benzaldehyde was consumed with a conversion of ~80% (Figure S17), further confirming the feasibility of benzaldehyde reduction. As mentioned earlier, both benzoin and deoxybenzoin are very useful commodity chemicals. However, in industry, either toxic catalysts and/or expensive reagents are required for the synthesis of benzoin and deoxybenzoin. For instance, benzoin is produced from the condensation of benzaldehyde, which is usually catalyzed by toxic CN⁻ or N-heterocyclic carbene. 49-51 Deoxybenzoin is normally synthesized from benzene and phenylacetic acid utilizing AlCl3-catalyzed C-C coupling. Functionalization of phenylacetic acid to form phenylacetyl chloride is a prerequisite for this process and stoichiometric PCl3 or SOCl₂ as the chlorine source is needed. Even though alternative processes have been reported, they typically require expensive reagents or complex pre-functionalization steps. 5 Hence, our photocatalytic C-C coupling for the one-step synthesis of benzoin and deoxybenzoin represents a great advance in their green production if high selectivity for each product could be achieved.

In order to probe the impacts of potential intermediates on the overall photocatalytic C–C coupling of benzyl alcohol on $ZnIn_2S_4$, control experiments using two different scavengers, including HCOONa and $K_2S_2O_8$, were performed. HCOONa and $K_2S_2O_8$ can act as excited hole and excited electron scavengers, respectively. A short duration of 2 h photocatalysis was purposely designed to minimize the complete conversion of benzyl alcohol for these experiments. HPLC spectra before

and after photocatalysis are plotted in Figure S18, and the conversion of benzyl alcohol, yields of C-C coupling products, and benzaldehyde are compared in Figure 4a. The parent

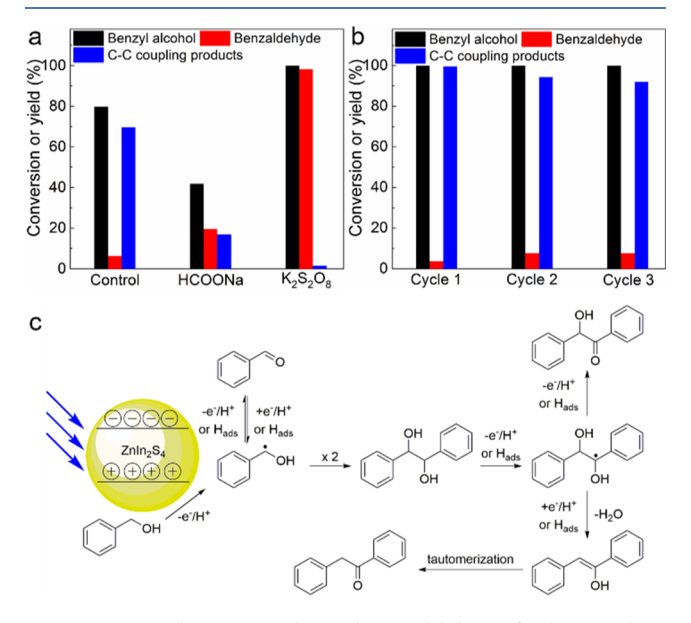


Figure 4. Mechanism study and recyclability of photocatalytic coupling of benzyl alcohol. (a) Conversion of benzyl alcohol and yields of benzaldehyde and C–C coupling products using different scavengers. Condition: 10 mM benzyl alcohol, 10 mM scavenger, 10 mg of $ZnIn_2S_4$, 3 mL of CH_3CN , 7 mL of H_2O , blue LED, 2 h. (b) Conversion of benzyl alcohol and yields of products using the same $ZnIn_2S_4$ catalyst for three consecutive photocatalysis cycles. Condition: 10 mM benzyl alcohol, 20 mg of $ZnIn_2S_4$, 3 mL of CH_3CN , 7 mL of H_2O , blue LED, 18 h. (c) Postulated reaction pathways from benzyl alcohol to benzoin and deoxybenzoin.

control experiment produced C-C coupling products with a total yield of 70% and benzyl alcohol conversion approached 80%. Upon the addition of HCOONa, benzyl alcohol conversion was substantially suppressed to 38%, demonstrating the necessity of excited hole in the transformation of benzyl alcohol. As a competent excited electron scavenger, K₂S₂O₈ is able to consume excited electrons very effectively. As clearly demonstrated in Figure 4a, the presence of K₂S₂O₈ almost completely suppressed the formation of C-C coupling products (yield: 2%), whereas benzaldehyde was produced with nearly unity yield and selectivity. This result is consistent with the fact that benzyl alcohol oxidation to benzaldehyde only requires excited holes, while excited electrons are critical for the formation of ketyl radicals (from the back reduction of benzaldehyde) and hence C-C coupling products. To further prove the generation of radicals, a radical trapping experiment was conducted using 1,1-diphenylethylene as a trapping reagent. Gas chromatography-mass spectrometry (GC-MS) spectra show only a small amount of hydrobenzoin (Figure S19), demonstrating that the addition of 1,1-diphenylethylene nearly inhibited its formation, further confirming a radicalinvolved mechanism for the photocatalytic benzyl alcohol C-C coupling. In addition, the direct detection of 1,3,3-triphenyl-1-propanol (Figures S19 and S20) proves that ketyl radicals were formed during photocatalysis. Overall, these control experiments with different scavengers and trapping reagent demonstrate that excited electrons/holes and radicals are all

ACS Catalysis pubs.acs.org/acscatalysis Research Article

crucial species for the success of photocatalytic C–C coupling reactions of benzyl alcohol achieved on $ZnIn_2S_4$.

Besides activity, robustness is another important parameter in assessing the performance of a photocatalyst. In particular, convenient recyclability is an additional advantage of solid-state photocatalysts relative to homogeneous counterparts. As displayed in Figures 4b and S21, after three consecutive photocatalysis cycles utilizing the same ZnIn₂S₄ photocatalyst, the yield of C–C coupling products was still higher than 90%. Post-photocatalysis XPS characterization (Figure S22) further confirmed the same composition and unchanged valence state of each element in ZnIn₂S₄ compared to the pristine sample. Overall, these results prove the excellent stability and recyclability of our ZnIn₂S₄ for long-term photocatalysis applications.

In addition, another control experiment was performed in CH_3CN/D_2O to investigate the hydrogen incorporation into the final C-C coupling products. Mass spectroscopy analysis (Figure S23) confirmed that no deuterium atoms were detected in benzoin, which was consistent with the nature of hydrogen abstraction of all steps toward the final formation of benzoin. However, the formation of deoxybenzoin requires the dehydration of hydrobenzoin and an enol intermediate is generated. The tautomerization from enol to deoxybenzoin may include hydrogen exchange with solvent D_2O , which eventually leads to the formation of deuterated deoxybenzoin.

Taking together all previous results, a plausible reaction pathway for the C-C coupling of benzyl alcohol on ZnIn₂S₄ is proposed in Figure 4c. Upon light irradiation, both excited electrons and holes are generated in ZnIn₂S₄. The nanosheet morphology of ZnIn₂S₄ allows fast migration of excitons to the photocatalyst surface. The oxidation power of excited holes will induce oxidation and deprotonation of benzyl alcohol and yield ketyl radicals, which could be further oxidized to benzaldehyde after subsequent oxidation and deprotonation. However, the newly formed benzaldehyde on the catalyst surface can be back reduced to ketyl radicals because the excited electrons of ZnIn₂S₄ have sufficient reducing power. Dimerization of the in situ generated ketyl radicals will lead to hydrobenzoin, which can be further consumed in two pathways: (i) oxidation and deprotonation to produce benzoin or (ii) dehydration to form deoxybenzoin.

As implied in the proposed mechanism, deoxybenzoin is a dehydration product of hydrobenzoin. It has been generally accepted that acidic environment would facilitate the dehydration process. 55,56 Hence, we reasoned that a small amount of acid might favor the formation of deoxybenzoin in the absence of water, which in turn would increase the selectivity of deoxybenzoin. Indeed, as shown in Figure 5a, with the addition of 1 equivalent of acetic acid, nearly complete consumption of benzyl alcohol was achieved within 2 h photocatalysis in pure acetonitrile, and hydrobenzoin was accumulated from the very beginning with a maximum yield of 65% at 1.5 h. Afterward, hydrobenzoin was consumed along with the increasing formation of deoxybenzoin whose final yield was 73%. The nuclear magnetic resonance (NMR) spectra collected before and post photocatalysis are compared in Figure S24. In contrast, upon the addition of water, which would suppress dehydration, the major product was benzoin with a yield of 83% (Figures 5b and S24). In addition, the main products can be easily separated from byproducts by column chromatography (Figure S25). These unprecedented high yields of benzoin and deoxybenzoin demonstrate that we were

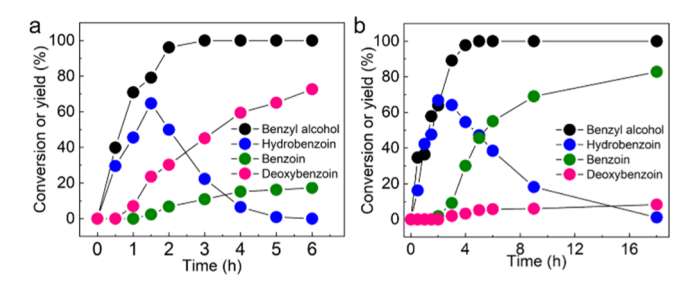


Figure 5. Photocatalytic coupling of benzyl alcohol. (a) Conversion of benzyl alcohol and yields of products over time during photocatalysis. Condition: 10 mM benzyl alcohol, 10 mM acetic acid, 10 mg of ZnIn₂S₄, 10 mL of CH₃CN, blue LED. (b) Conversion of benzyl alcohol and yields of products over time during photocatalysis. Condition: 10 mM benzyl alcohol, 10 mM acetic acid, 10 mg of ZnIn₂S₄, 7 mL of CH₃CN, 3 mL of H₂O, blue LED.

able to produce industrially important feedstock chemicals with high selectivity via judiciously modulating the photocatalytic conditions.

Our proposed mechanism (Figure 4c) implies the presence of a hydrogen pool on the photocatalyst surface, which is beneficial for the back reduction of benzaldehyde to ketyl radical. Hence, we reason that if a hydrogen evolution cocatalyst exists on ZnIn₂S₄, H₂ production will take place more efficiently and the final organic product should remain as benzaldehyde. With this hypothesis in mind, we prepared Ni/ ZnIn₂S₄ as a new photocatalyst because Ni is an excellent H₂ evolution catalyst 57,58 and assessed its activity toward the photocatalytic transformation of benzyl alcohol and H₂ evolution. The XPS spectra of Ni/ZnIn₂S₄ are included in Figure S26, confirming the anticipated composition and valence state of each element in Ni/ZnIn₂S₄. ^{59,60} Inductively coupled plasma (ICP)-atomic emission spectroscopy measurement indicates 2 wt % Ni in Ni/ZnIn₂S₄ (Table S2). Figure 6a plots the conversion of benzyl alcohol and yields of

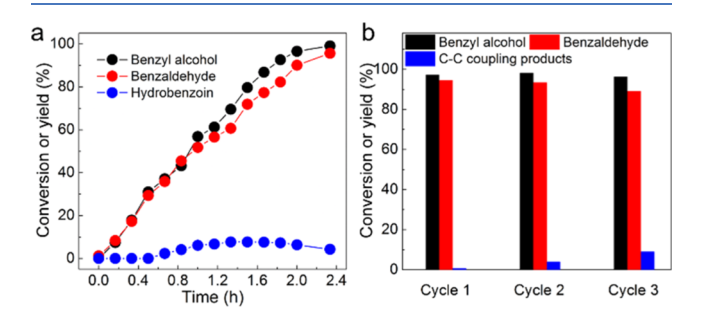


Figure 6. Photocatalytic oxidation of benzyl alcohol. (a) Evolution of benzyl alcohol conversion and yields of benzaldehyde and hydrobenzoin during photocatalysis. Condition: 10 mM benzyl alcohol, 10 mg of Ni/ZnIn₂S₄, 3 mL of CH₃CN, 7 mL of H₂O, blue LED. (b) Benzyl alcohol conversion and yields of benzaldehyde and hydrobenzoin for three consecutive photocatalysis cycles using the same Ni/ZnIn₂S₄ photocatalyst. Condition: 10 mM benzyl alcohol, 20 mg of Ni/ZnIn₂S₄, 3 mL of CH₃CN, 7 mL of H₂O, blue LED, 2.4 h.

benzaldehyde and hydrobenzoin over time using $Ni/ZnIn_2S_4$ as the photocatalyst. It is apparent that nearly quantitative transformation of benzyl alcohol to benzaldehyde was observed and the yield of hydrobenzoin remained very low. The corresponding HPLC and 1H NMR spectra of this photocatalysis could be found in Figures S27 and S28. Also, a quantitative amount of H_2 was generated during this process

(Figure S29). In addition, Ni/ZnIn₂S₄ demonstrated robust stability for long-term photocatalysis. As shown in Figures 6b and S30, three consecutive photocatalysis processes using the same Ni/ZnIn₂S₄ only resulted in modest decrease in benzaldehyde yield which remained as ~90% after three cycles. Post-photocatalysis XPS characterization (Figure S31) further verified the robustness of Ni/ZnIn₂S₄. Besides metallic Ni, NiS is also an efficient cocatalyst for H₂ production. Therefore, to further confirm the effect of the cocatalyst, another control experiment was conducted utilizing NiS/ZnIn₂S₄ as the photocatalyst. Similar to Ni/ZnIn₂S₄, NiS/ZnIn₂S₄ exhibited an excellent activity for benzyl alcohol upgrading with nearly quantitative yields of benzaldehyde and H₂ production (Figure S32).

The above success of photocatalytic C-C coupling reactions of aromatic aldehydes and alcohols prompt us to expand its practical applications, such as production of value-added chemicals and fuels from sustainable carbon source (e.g., biomass). Among many biomass-derived platform chemicals, furfural is one of the few examples which have been produced on an industrial scale and exhibits great potential for the production of biofuels. ^{62–67} Wang et al. recently reported that photocatalytic conversion of a furfural-derived molecule, 2methylfuran, on Ru/ZnIn₂S₄ was able to produce a mixture of furan-incorporated dimers, trimers, and tetramers, which can act as diesel fuel precursors. 63 Subsequent deoxyhydrogenation of these diesel fuel precursors led to the formation of a mixture of hydrocarbons with carbon numbers in the range of C10 to C20. However, 2-methylfuran itself is a downstream deoxyhydrogenation product of furfural, and it has not been produced on an industrial scale yet. Furthermore, the slow reaction rate and mediocre yields of 2-methylfuran coupling products render this approach less attractive for practical applications. Therefore, it is more appealing to attempt direct coupling of furfural (or its one-step products) to produce biofuels, ideally with well-controlled carbon length. Encouraged by our photocatalytic C-C coupling results obtained on ZnIn₂S₄, we first assessed the possibility of photocatalytic furfural homocoupling in the presence of a sacrificial electron donor, TEA. The ¹H NMR spectra shown in Figure 7 demonstrate that furfural could be completely coupled to yield hydrofuroin as the final product. In addition, TEA could be further replaced by furfural alcohol (a one-step product of furfural). Equivalent addition of furfural and furfural alcohol in the photocatalysis solution also resulted in the formation of hydrofuroin with a yield above 90%. Mass analysis also indicates the formation of furoin and deoxyfuroin (Figure S33) as minor products. The hydrofuroin yield over time exhibited a rapid reaction rate during the initial 4 h with a yield of ~56% (Figures S34 and S35). Moreover, a large-scale production of hydrofuroin from the heterocoupling between furfural alcohol and furfural was realized with an isolated yield of ~75% (Figure S36). It has been demonstrated that a one-step deoxyhydrogenation of hydrofuroin will yield C₁₀H₂₂ as the final product with high yield (>85%), which falls in the middle of the carbon range of jet fuels (C5 to C16).61

CONCLUSIONS

In conclusion, we have reported that ${\rm ZnIn_2S_4}$ nanosheets are very effective in promoting photocatalytic homocoupling of benzaldehyde with the aid of a sacrificial electron donor (e.g., TEA). We further demonstrated that it was feasible to circumvent the employment of TEA and the photocatalytic

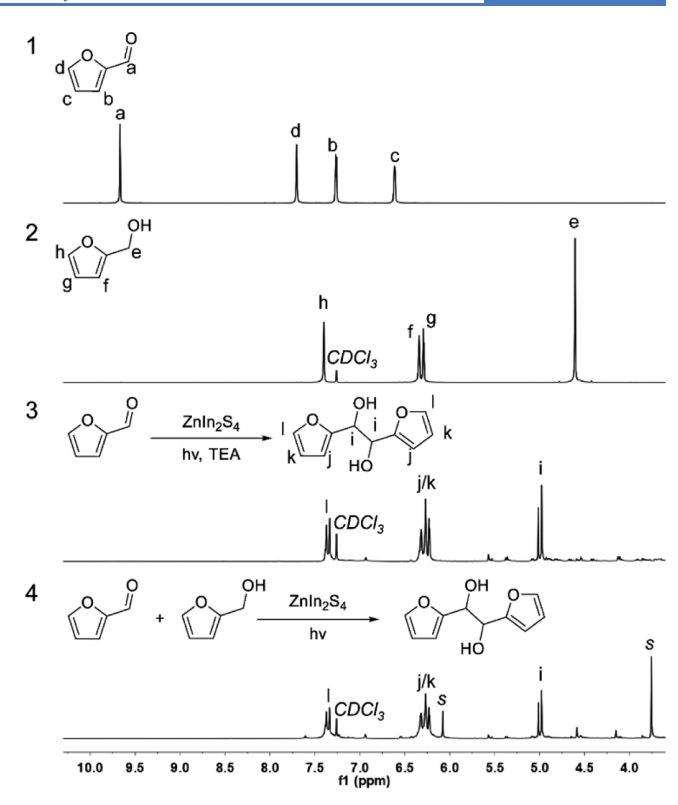


Figure 7. ¹H NMR spectra of photocatalytic homocoupling of furfural and heterocoupling of furfural and furfural alcohol. ¹H NMR spectra of (1) furfural, (2) furfural alcohol, (3) products from furfural homocoupling (condition: 10 mM furfural, 10 mg of ZnIn₂S₄, 9 mL of CH₃CN, 1 mL of H₂O, 1 mL of TEA, blue LED, 4 h), and (4) products from furfural and furfural alcohol heterocoupling (condition: 10 mM furfural, 10 mM furfural alcohol, 1 mM 1,3,5-trimethoxyl benzene as the internal standard (labeled as "s"), 10 mg of ZnIn₂S₄, 9 mL of CH₃CN, 1 mL of H₂O, blue LED, 16 h).

C-C coupling could be equally achieved on ZnIn₂S₄ when benzyl alcohol was used as the starting substrate. The critical species, including excited electrons, excited holes, ketyl radicals, and adsorbed hydrogen pool are crucial for the success of its C-C bond formation. Furthermore, unprecedented yields of industrially important feedstock chemicals, benzoin and deoxybenzoin, could be formed with high selectivity through fine tuning of the photocatalytic conditions. Finally, our photocatalytic C-C coupling strategy was extended to transform a biomass-derived platform chemical, furfural, to a jet fuel precursor, hydrofuroin. Not only homocoupling of furfural could be realized on ZnIn₂S₄ with the assistance of TEA but also heterocoupling between furfural and furfural alcohol was also able to produce the desirable C-C coupling products in the absence of any sacrificial reagents, highlighting the promise of our semiconductor-based photocatalytic C-C coupling in practical applications.

EXPERIMENTAL SECTION

Synthesis of ZnIn₂S₄. ZnIn₂S₄ was synthesized following a microwave-assisted method. Briefly, 0.0595 g of Zn(NO₃)₂· $6H_2O$, 0.1203 g of In(NO₃)· xH_2O , and 0.1202 g of thioacetamide were dissolved in 20 mL of water. The solution was adjusted to pH 2.5 with the addition of 0.5 M HNO₃. The resulting solution was subjected to microwave treatment at a certain temperature (80, 90, 100, 110, 120, and 130 °C) for 10 min. Subsequently, the prepared ZnIn₂S₄ was washed with

water and methanol thoroughly via centrifugation and dried under vacuum at room temperature.

Synthesis of Ni/Znln₂S₄. A simple chemical reduction method was applied to the synthesis of Ni-loaded $ZnIn_2S_4$ (Ni/ZnIn₂S₄). Specifically, 80 mg of $ZnIn_2S_4$ was dispersed in a NiCl₂ (6.7 mg) solution (18 mL). After ultrasonication for 30 min, the above suspension was mixed with a 2 mL solution containing 0.4 M NaBH₄ and 2.5 M NaOH, followed by stirring at room temperature for 1 h. The synthesized Ni/ZnIn₂S₄ was collected by centrifugation, washed with water and methanol thoroughly, and dried under vacuum at room temperature.

Synthesis of NiS/ZnIn₂S₄. A modified hydrothermal method was applied to the preparation of NiS/ZnIn₂S₄. ⁶¹ 0.08 g of ZnIn₂S₄, 7 mg of Ni(OCOCH₃)₂·4H₂O, and 2.1 mg of thioacetamide were dispersed in 20 mL of deionized H₂O by stirring and ultrasonication for 1 h. The above suspension was transferred to a 40 mL Teflon autoclave and heated at 120 °C for 4 h. The final solid was collected by centrifugation, washed with water and methanol thoroughly, and dried under vacuum at room temperature.

Physical Method. SEM (FEI XL30, 15 kV) was used to characterize photocatalyst samples. A scanning electron microscope (FEI Talos F200X) equipped with super-EDX operating at 200 kV was used to conduct element mapping. XRD patterns were collected on a Philips X'Pert Pro PW3040/00 (PAN 2 Analytical) instrument. The scan range was set from 10 to 90° (in 2θ) with a Cu-tube operated at 45 kV and 40 mA. XPS measurements were carried out on an X-ray photoelectron spectrometer (K-alpha, Thermo Fisher Scientific, USA) using a monochromatic Al K α X-ray source. C 1s peak at 284.6 eV was used as an internal standard for spectral calibration. Each sample was sputtered by 1 keV Ar⁺ for 60 s to remove adventitious contaminants on the surface.

Photocatalytic Experiments. Generally, a mixture of 10 mg of photocatalyst, 10 mM organic substrate, and 10 mL of solvent were added in a sealed 25 mL round-bottom flask. After ultrasonication for 30 min, the mixture was bubbled with N_2 for 10 min. Subsequently, the suspension was irradiated under royal blue light (λ_{irr} = 440–460 nm) using an 8 W lightemitting diode (LED) (SinkPAD-II, Luxeon Star LEDs) for a certain period of time. For scavenger control experiments, the concentration of each scavenger was 10 mM.

Radical Trapping Experiments. Based on the literature,³¹ 1,1-diphenylethylene was applied to trap the radical intermediates in photocatalytic benzyl alcohol transformation. Briefly, 5 mmol 1,1-diphenylethylene, 2.5 mmol benzyl alcohol, 50 mg of ZnIn₂S₄, and 25 mL of acetonitrile were added in a sealed 100 mL round-bottom flask. After ultrasonication for 30 min, the mixture was bubbled with N_2 for 20 min. Subsequently, the suspension was stirred and irradiated under royal blue light (λ_{irr} = 440–460 nm) using an 8 W LED (SinkPAD-II, Luxeon Star LEDs) for 60 h. Subsequently, the reaction mixture was centrifuged and washed to remove the catalyst. A small amount of the liquid mixture (50 μ L) was diluted in acetonitrile (1.5 mL) and analyzed via GC-MS. For the other liquid portion, the solvent was evaporated and the reaction mixture was purified on silica gel (eluent: hexane/ ethyl acetate = 10/1).

Product Quantification. HPLC on an Agilent Technologies 1260 Infinity II at 25 °C was used to analyze organic products. The HPLC was equipped with an ultraviolet—visible detector and a 4.6 mm \times 150 mm Shim-pack GWS 5 μ m C18

column. A mixture of eluting solvents (A: 5 mM ammonium acetate aqueous solution and B: CH₃CN) was utilized. The elution was composed of 40% A and 60% B for 11 min run time, and the flow rate was 0.5 mL min $^{-1}$. The products were identified and quantified from the calibration curves of standard chemical solutions. The $^{1}\mathrm{H}$ NMR spectra were measured on a Bruker Advance III HD Ascend 400 Hz NMR. GC–MS were measured on MassHunter for Agilent GC–MS with standard electron impact sources. The temperature was set from 70 °C (1 min) to 280 °C (1 min) with a ramp rate of 15 °C/min.

ASSOCIATED CONTENT

Supporting Information

The Supporting Information is available free of charge at https://pubs.acs.org/doi/10.1021/acscatal.0c01715.

Additional condition optimization table, XPS, HPLC, ¹H NMR, GC-MS, and ICP (PDF)

AUTHOR INFORMATION

Corresponding Author

Yujie Sun — Department of Chemistry, University of Cincinnati, Cincinnati, Ohio 45221, United States; ⊙ orcid.org/0000-0002-4122-6255; Email: yujie.sun@uc.edu

Authors

Guanqun Han — Department of Chemistry, University of Cincinnati, Cincinnati, Ohio 45221, United States

Xingwu Liu — Syncat@Beijing, Synfuels CHINA Company, Ltd.,
Beijing 101407, China; ⊙ orcid.org/0000-0002-8564-1151

Zhi Cao — Syncat@Beijing, Synfuels CHINA Company, Ltd.,
Beijing 101407, China; State Key Laboratory of Coal
Conversion, Institute of Coal Chemistry, Chinese Academy of
Sciences, Taiyuan 030001, China; ⊙ orcid.org/0000-00021050-2165

Complete contact information is available at: https://pubs.acs.org/10.1021/acscatal.0c01715

Author Contributions

The manuscript was written through contributions of all authors.

Notes

The authors declare no competing financial interest.

ACKNOWLEDGMENTS

Y.S. acknowledges the financial support of Herman Frasch Foundation (820-HF17), National Science Foundation (CHE-1914546), and the University of Cincinnati. Z.C. acknowledges the National Natural Science Foundation of China (no. 21972161), Chinese Academy of Sciences (CAS) Pioneer Talents Program (no. 2018–095), Shanxi Talent Program (no. 2019SBRJH01), Autonomous Research Project of State Key Laboratory of Coal Conversion (SKLCC) (no. 2020BWZ006), Institute of Coal Chemistry (ICC) Innovation Fund (no. 2019SC001), University of Chinese Academy of Sciences, and Synfuels China, Co. Ltd. for financial support. NMR experiments were performed on a Bruker AVANCE NEO 400 MHz NMR spectrometer (funded by NSF-MRI grant CHE-1726092).

ACS Catalysis pubs.acs.org/acscatalysis Research Article

REFERENCES

- (1) Cherney, A. H.; Kadunce, N. T.; Reisman, S. E. Enantioselective and Enantiospecific Transition-Metal-Catalyzed Cross-Coupling Reactions of Organometallic Reagents To Construct C–C Bonds. *Chem. Rev.* **2015**, *115*, 9587–9652.
- (2) Xie, J.; Jin, H.; Hashmi, A. S. K. The Recent Achievements of Redox-Neutral Radical C-C Cross-Coupling Enabled by Visible-Light. *Chem. Soc. Rev.* **2017**, *46*, 5193–5203.
- (3) Jana, R.; Pathak, T. P.; Sigman, M. S. Advances in Transition Metal (Pd,Ni,Fe)-Catalyzed Cross-Coupling Reactions Using Alkylorganometallics as Reaction Partners. *Chem. Rev.* **2011**, *111*, 1417–1492.
- (4) Yeh, C.-H.; Korivi, R. P.; Cheng, C.-H. Ene-Carbonyl Reductive Coupling Mediated by Zinc and Ammonia for the Synthesis of γ -Hydroxybutyric Acid Derivatives. *Adv. Synth. Catal.* **2013**, 355, 1338–1344
- (5) Paradas, M.; Campaña, A. G.; Estévez, R. E.; Álvarez de Cienfuegos, L.; Jiménez, T.; Robles, R.; Cuerva, J. M.; Oltra, J. E. Unexpected Ti^{III}/Mn-Promoted Pinacol Coupling of Ketones. *J. Org. Chem.* **2009**, *74*, 3616–3619.
- (6) Hirao, T.; Hatano, B.; Imamoto, Y.; Ogawa, A. A Catalytic System Consisting of Vanadium, Chlorosilane, and Aluminum Metal in the Stereoselective Pinacol Coupling Reaction of Benzaldehyde Derivatives. *J. Org. Chem.* **1999**, *64*, 7665–7667.
- (7) McMurry, J. E. Carbonyl-Coupling Reactions Using Low-Valent Titanium. *Chem. Rev.* **1989**, *89*, 1513–1524.
- (8) Edmonds, D. J.; Johnston, D.; Procter, D. J. Samarium(II)-Iodide-Mediated Cyclizations in Natural Product Synthesis. *Chem. Rev.* **2004**, *104*, 3371–3404.
- (9) Huynh, M. H. V.; Meyer, T. J. Proton-Coupled Electron Transfer. Chem. Rev. 2007, 107, 5004-5064.
- (10) Tarantino, K. T.; Liu, P.; Knowles, R. R. Catalytic Ketyl-Olefin Cyclizations Enabled by Proton-Coupled Electron Transfer. *J. Am. Chem. Soc.* **2013**, *135*, 10022–10025.
- (11) Rono, L. J.; Yayla, H. G.; Wang, D. Y.; Armstrong, M. F.; Knowles, R. R. Enantioselective Photoredox Catalysis Enabled by Proton-Coupled Electron Transfer: Development of An Asymmetric Aza-Pinacol Cyclization. J. Am. Chem. Soc. 2013, 135, 17735–17738.
- (12) Petronijević, F. R.; Nappi, M.; MacMillan, D. W. C. Direct β -functionalization of cyclic ketones with aryl ketones via the merger of photoredox and organocatalysis. *J. Am. Chem. Soc.* **2013**, *135*, 18323–18326.
- (13) Wang, C.; Qin, J.; Shen, X.; Riedel, R.; Harms, K.; Meggers, E. Asymmetric Radical-Radical Cross-Coupling through Visible-Light-Activated Iridium Catalysis. *Angew. Chem., Int. Ed.* **2016**, *55*, 685–688
- (14) Twilton, J.; Christensen, M.; DiRocco, D. A.; Ruck, R. T.; Davies, I. W.; MacMillan, D. W. C. Selective Hydrogen Atom Abstraction through Induced Bond Polarization: Direct α -Arylation of Alcohols through Photoredox, HAT, and Nickel Catalysis. *Angew. Chem., Int. Ed.* **2018**, *57*, 5369–5373.
- (15) Jeffrey, J. L.; Terrett, J. A.; MacMillan, D. W. C. O–H hydrogen bonding promotes H-atom transfer from C–H bonds for C-alkylation of alcohols. *Science* **2015**, 349, 1532–1536.
- (16) Lee, K. N.; Lei, Z.; Ngai, M.-Y. β -Selective Reductive Coupling of Alkenylpyridines with Aldehydes and Imines via Synergistic Lewis Acid/Photoredox Catalysis. *J. Am. Chem. Soc.* **2017**, *139*, 5003–5006.
- (17) Matsuoka, S.; Kohzuki, T.; Kuwana, Y.; Nakamura, A.; Yanagida, S. Visible-light-induced photocatalysis of poly(pyridine-2,5-diyl). Photoreduction of water, carbonyl compounds and alkenes with triethylamine. *J. Chem. Soc., Perkin Trans.* 2 **1992**, 679–685.
- (18) Nakajima, M.; Fava, E.; Loescher, S.; Jiang, Z.; Rueping, M. Photoredox-Catalyzed Reductive Coupling of Aldehydes, Ketones, and Imines with Visible Light. *Angew. Chem., Int. Ed.* **2015**, *54*, 8828–8832.
- (19) Hao, M.; Deng, X.; Xu, L.; Li, Z. Noble Metal Free MoS₂/ZnIn₂S₄ Nanocomposite for Acceptorless Photocatalytic Semi-Dehydrogenation of 1,2,3,4-Tetrahydroisoquinoline to Produce 3,4-Dihydroisoquinoline. *Appl. Catal., B* **2019**, 252, 18–23.

- (20) Wang, B.; Deng, Z.; Fu, X.; Xu, C.; Li, Z. Photodeposition of Pd Nanoparticles on $ZnIn_2S_4$ for Efficient Alkylation of Amines and Ketones' α -H with Alcohols under Visible Light. *Appl. Catal., B* **2018**, 237, 970–975.
- (21) Li, Y.; Cai, J.; Hao, M.; Li, Z. Visible Light Initiated Hydrothiolation of Alkenes and Alkynes over ZnIn₂S₄. *Green Chem.* **2019**, 21, 2345–2351.
- (22) Caputo, J. A.; Frenette, L. C.; Zhao, N.; Sowers, K. L.; Krauss, T. D.; Weix, D. J. General and Efficient C-C Bond Forming Photoredox Catalysis with Semiconductor Quantum Dots. *J. Am. Chem. Soc.* **2017**, *139*, 4250–4253.
- (23) Chakraborty, I. N.; Roy, S.; Devatha, G.; Rao, A.; Pillai, P. P. InP/ZnS Quantum Dots as Efficient Visible-Light Photocatalysts for Redox and Carbon-Carbon Coupling Reactions. *Chem. Mater.* **2019**, *31*, 2258–2262.
- (24) Han, G.; Yan, T.; Zhang, W.; Zhang, Y. C.; Lee, D. Y.; Cao, Z.; Sun, Y. Highly Selective Photocatalytic Valorization of Lignin Model Compounds Using Ultrathin Metal/CdS. ACS Catal. 2019, 9, 11341–11340
- (25) You, B.; Han, G.; Sun, Y. Electrocatalytic and Photocatalytic Hydrogen Evolution Integrated with Organic Oxidation. *Chem. Commun.* **2018**, *54*, 5943–5955.
- (26) Cao, B. Y.; Xu, S.; Ren, Y. L.; Yu, Y.; Guo, J. Y.; Zhang, L.; Li, N.; Zhang, G. C.; Zhou, C. S. Photocatalytic Hydrogenation Coupling of Acetone into Pinacol Using Formic Acid as Hydrogen Source. *Chem. Lett.* **2017**, *46*, 1773–1776.
- (27) Wang, Y.; Ren, P.; Gu, X.; Wen, X.; Wang, Y.; Guo, X.; Waclawik, E. R.; Zhu, H.; Zheng, Z. Probing the mechanism of benzaldehyde reduction to chiral hydrobenzoin on the CNT surface under near-UV light irradiation. *Green Chem.* **2016**, *18*, 1482–1487.
- (28) Manley, D.; Buzzetti, L.; MacKessack-Leitch, A.; Walton, J. Hydrogenations without Hydrogen: Titania Photocatalyzed Reductions of Maleimides and Aldehydes. *Molecules* **2014**, *19*, 15324–15338.
- (29) Griesbeck, A. G.; Reckenthäler, M. Homogeneous and Heterogeneous Photoredox-Catalyzed Hydroxymethylation of Ketones and Keto Esters: Catalyst Screening, Chemoselectivity and Dilution Effects. *Beilstein J. Org. Chem.* **2014**, *10*, 1143–1150.
- (30) McClelland, K. P.; Weiss, E. A. Selective Photocatalytic Oxidation of Benzyl Alcohol to Benzaldehyde or C-C Coupled Products by Visible-Light-Absorbing Quantum Dots. *ACS Appl. Energy Mater.* **2019**, 2, 92–96.
- (31) Luo, N.; Hou, T.; Liu, S.; Zeng, B.; Lu, J.; Zhang, J.; Li, H.; Wang, F. Photocatalytic Coproduction of Deoxybenzoin and H₂ through Tandem Redox Reactions. *ACS Catal.* **2020**, *10*, 762–769.
- (32) Sun, X.; Jiang, D.; Zhang, L.; Wang, W. Alkaline Modified g- C_3N_4 Photocatalyst for High Selective Oxide Coupling of Benzyl Alcohol to Benzoin. *Appl. Catal.*, B **2018**, 220, 553–560.
- (33) Mitkina, T.; Stanglmair, C.; Setzer, W.; Gruber, M.; Kisch, H.; König, B. Visible light mediated homo- and heterocoupling of benzyl alcohols and benzyl amines on polycrystalline cadmium sulfide. *Org. Biomol. Chem.* **2012**, *10*, 3556–3561.
- (34) Okano, K. Synthesis and Application of Chiral Hydrobenzoin. *Tetrahedron* **2011**, *67*, 2483–2512.
- (35) Zhang, G.; Yang, S.; Zhang, X.; Lin, Q.; Das, D. K.; Liu, J.; Fang, X. Dynamic Kinetic Resolution Enabled by Intramolecular Benzoin Reaction: Synthetic Applications and Mechanistic Insights. *J. Am. Chem. Soc.* **2016**, *138*, 7932–7938.
- (36) Frick, E.; Schweigert, C.; Noble, B. B.; Ernst, H. A.; Lauer, A.; Liang, Y.; Voll, D.; Coote, M. L.; Unterreiner, A.-N.; Barner-Kowollik, C. Toward a Quantitative Description of Radical Photoinitiator Structure-Reactivity Correlations. *Macromolecules* **2016**, *49*, 80–89.
- (37) Kabalka, G. W.; Ju, Y.; Wu, Z. A New Titanium Tetrachloride Mediated Annulation of α -Aryl-Substituted Carbonyl Compounds with Alkynes: A Simple and Highly Efficient Method for the Regioselective Synthesis of Polysubstituted Naphthalene Derivatives. *J. Org. Chem.* **2003**, *68*, 7915–7917.

- (38) Kim, Y.-W.; Brueggemeier, R. W. A convenient one-pot synthesis of 2-(alkylthio)isoflavones from deoxybenzoins using a phase transfer catalyst. *Tetrahedron Lett.* **2002**, *43*, 6113–6115.
- (39) Gupton, J. T.; Clough, S. C.; Miller, R. B.; Lukens, J. R.; Henry, C. A.; Kanters, R. P. F.; Sikorski, J. A. The application of vinylogous iminium salt derivatives to the synthesis of Ningalin B hexamethyl ether. *Tetrahedron* **2003**, *59*, 207–215.
- (40) Churruca, F.; SanMartin, R.; Tellitu, I.; Domínguez, E. Palladium-Catalyzed Arylation of Ketone Enolates: An Expeditious Entry to Tamoxifen-Related 1,2,2-Triarylethanones. *Org. Lett.* **2002**, *4*, 1591–1594.
- (41) Vaipolin, A. A.; Nikolaev, Y. A.; Rud', V. Y.; Rud', Y. V.; Terukov, E. I.; Fernelius, N. Fabrication and Properties of Photosensitive Structures Based on ZnIn₂S₄ Single Crystals. *Semiconductors* **2003**, *37*, 178–182.
- (42) Chai, B.; Peng, T.; Zeng, P.; Zhang, X. Preparation of A MWCNTs/ZnIn₂S₄ Composite and Its Enhanced Photocatalytic Hydrogen Production under Visible-Light Irradiation. *Dalton Trans.* **2012**, *41*, 1179–1186.
- (43) Ye, L.; Li, Z. ZnIn₂S₄: A Photocatalyst for the Selective Aerobic Oxidation of Amines to Imines under Visible Light. *ChemCatChem* **2014**, *6*, 2540–2543.
- (44) Xu, L.; Deng, X.; Li, Z. Photocatalytic Splitting of Thiols to Produce Disulfides and Hydrogen over PtS/ZnIn₂S₄ Nanocomposites under Visible Light. *Appl. Catal., B* **2018**, 234, 50–55.
- (45) Chen, Z.; Li, D.; Zhang, W.; Chen, C.; Li, W.; Sun, M.; He, Y.; Fu, X. Low-Temperature and Template-Free Synthesis of ZnIn₂S₄ Microspheres. *Inorg. Chem.* **2008**, *47*, 9766–9772.
- (46) Chen, Z.; Li, D.; Xiao, G.; He, Y.; Xu, Y.-J. Microwave-Assisted Hydrothermal Synthesis of Marigold-like ZnIn₂S₄ Microspheres and Their Visible Light Photocatalytic Activity. *J. Solid State Chem.* **2012**, 186, 247–254.
- (47) Kisch, H. Semiconductor Photocatalysis for Organic Synthesis. *Adv. Photochem.* **2007**, *26*, 93–143.
- (48) Luo, N.; Wang, M.; Li, H.; Zhang, J.; Hou, T.; Chen, H.; Zhang, X.; Lu, J.; Wang, F. Visible-Light-Driven Self-Hydrogen Transfer Hydrogenolysis of Lignin Models and Extracts into Phenolic Products. ACS Catal. 2017, 7, 4571–4580.
- (49) Marion, N.; Díez-González, S.; Nolan, S. P. N-Heterocyclic Carbenes as Organocatalysts. *Angew. Chem., Int. Ed.* **2007**, *46*, 2988–3000
- (50) Matsubara, R.; Kobayashi, S. Enamides and Enecarbamates as Nucleophiles in Stereoselective C-C and C-N Bond-Forming Reactions. *Acc. Chem. Res.* **2008**, *41*, 292–301.
- (51) He, Y.; Xue, Y. Mechanism Insight into the Cyanide-Catalyzed Benzoin Condensation: A Density Functional Theory Study. *J. Phys. Chem. A* **2010**, *114*, 9222–9230.
- (52) Miao, T.; Wang, G.-W. Synthesis of Ketones by Palladium-Catalysed Desulfitative Reaction of Arylsulfinic Acids with Nitriles. *Chem. Commun.* **2011**, 47, 9501–9503.
- (53) Ding, Y.; Zhang, W.; Li, H.; Meng, Y.; Zhang, T.; Chen, Q.-Y.; Zhu, C. Metal-Free Synthesis of Ketones by Visible-Light Induced Aerobic Oxidative Radical Addition of Aryl Hydrazines to Alkenes. *Green Chem.* 2017, 19, 2941–2944.
- (54) Chen, X.; Chen, Z.; So, C. M. Exploration of Aryl Phosphates in Palladium-Catalyzed Mono-α-arylation of Aryl and Heteroaryl Ketones. *J. Org. Chem.* **2019**, *84*, 6337–6346.
- (55) van Putten, R.-J.; van der Waal, J. C.; de Jong, E.; Rasrendra, C. B.; Heeres, H. J.; de Vries, J. G. Hydroxymethylfurfural, A Versatile Platform Chemical Made from Renewable Resources. *Chem. Rev.* **2013**, *113*, 1499–1597.
- (56) Mika, L. T.; Cséfalvay, E.; Németh, Á. Catalytic Conversion of Carbohydrates to Initial Platform Chemicals: Chemistry and Sustainability. *Chem. Rev.* **2018**, *118*, 505–613.
- (57) Jiang, N.; Tang, Q.; Sheng, M.; You, B.; Jiang, D.-e.; Sun, Y. Nickel Sulfides for Electrocatalytic Hydrogen Evolution under Alkaline Conditions: A Case Study of Crystalline NiS, NiS₂, and Ni₃S₂ Nanoparticles. *Catal. Sci. Technol.* **2016**, *6*, 1077–1084.

- (58) You, B.; Liu, X.; Liu, X.; Sun, Y. Efficient H₂ Evolution Coupled with Oxidative Refining of Alcohols via a Hierarchically Porous Nickel Bifunctional Electrocatalyst. *ACS Catal.* **2017**, *7*, 4564–4570.
- (59) You, B.; Jiang, N.; Sheng, M.; Bhushan, M. W.; Sun, Y. Hierarchically Porous Urchin-like $\mathrm{Ni_2P}$ Superstructures Supported on Nickel Foam as Efficient Bifunctional Electrocatalysts for Overall Water Splitting. ACS Catal. 2015, 6, 714–721.
- (60) Pan, Y.; Liu, Y.; Zhao, J.; Yang, K.; Liang, J.; Liu, D.; Hu, W.; Liu, D.; Liu, Y.; Liu, C. Monodispersed Nickel Phosphide Nanocrystals with Different Phases: Synthesis, Characterization and Electrocatalytic Properties for Hydrogen Evolution. *J. Mater. Chem. A* **2015**, *3*, 1656–1665.
- (61) Wei, L.; Chen, Y.; Zhao, J.; Li, Z. Preparation of NiS/ZnIn₂S₄ as a Superior Photocatalyst for Hydrogen Evolution under Visible Light Irradiation. *Beilstein J. Nanotechnol.* **2013**, *4*, 949–955.
- (62) Zang, H.; Wang, K.; Zhang, M.; Xie, R.; Wang, L.; Chen, E. Y.-X. Catalytic Coupling of Biomass-Derived Aldehydes into Intermediates for Biofuels and Materials. *Catal. Sci. Technol.* **2018**, *8*, 1777–1798.
- (63) Luo, N.; Montini, T.; Zhang, J.; Fornasiero, P.; Fonda, E.; Hou, T.; Nie, W.; Lu, J.; Liu, J.; Heggen, M.; Lin, L.; Ma, C.; Wang, M.; Fan, F.; Jin, S.; Wang, F. Visible-Light-Driven Coproduction of Diesel Precursors and Hydrogen from Lignocellulose-Derived Methylfurans. *Nat. Energy* **2019**, *4*, 575–584.
- (64) You, B.; Liu, X.; Jiang, N.; Sun, Y. A General Strategy for Decoupled Hydrogen Production from Water Splitting by Integrating Oxidative Biomass Valorization. *J. Am. Chem. Soc.* **2016**, *138*, 13639—13646
- (65) Jiang, N.; You, B.; Boonstra, R.; Terrero Rodriguez, I. M.; Sun, Y. Integrating Electrocatalytic 5-Hydroxymethylfurfural Oxidation and Hydrogen Production via Co–P-Derived Electrocatalysts. *ACS Energy Lett.* **2016**, *1*, 386–390.
- (66) You, B.; Jiang, N.; Liu, X.; Sun, Y. Simultaneous H_2 Generation and Biomass Upgrading in Water by an Efficient Noble-Metal-Free Bifunctional Electrocatalyst. *Angew. Chem., Int. Ed.* **2016**, *55*, 9913–9917
- (67) Han, G.; Jin, Y.-H.; Burgess, R. A.; Dickenson, N. E.; Cao, X.-M.; Sun, Y. Visible-Light-Driven Valorization of Biomass Intermediates Integrated with H₂ Production Catalyzed by Ultrathin Ni/CdS Nanosheets. *J. Am. Chem. Soc.* **2017**, *139*, 15584–15587.
- (68) Huang, Y.-B.; Yang, Z.; Dai, J.-J.; Guo, Q.-X.; Fu, Y. Production of high quality fuels from lignocellulose-derived chemicals: a convenient C–C bond formation of furfural, 5-methylfurfural and aromatic aldehyde. *RSC Adv.* **2012**, *2*, 11211–11214.